Available online at www.sciencedirect.com
SCIENCE DIRECT®
Optical Materials xxx (2004) xxx–xxx
OPTICAL Materials
www.elsevier.com/locate/optmat

Optical-telecommunication-band fluorescence properties of Er^{3+}-doped YAG nanocrystals synthesized by glycothermal method

Masayuki Nishi [a,*], Setsuhisa Tanabe [b,**], Masashi Inoue [c], Masaru Takahashi [c], Koji Fujita [a], Kazuyuki Hirao [a]

[a] Department of Material Chemistry, Graduate School of Engineering, Kyoto University, Nishikyo-ku, Kyoto 615-8510, Japan
[b] Graduate School of Human and Environmental Studies, Kyoto University, Sakyo-ku, Kyoto 606-8501, Japan
[c] Department of Energy and Hydrocarbon Chemistry, Graduate School of Engineering Kyoto University, Nishikyo-ku, Kyoto 615-8510, Japan

Received 30 July 2004; accepted 31 August 2004

Abstract

Er^{3+}-doped YAG (Er:YAG) nanocrystals were prepared by a glycothermal synthesis, and the effect of heat-treatment on the size of the nanocrystals and their fluorescence properties in optical-telecommunication-band were examined. The crystallite size of the as-prepared nanocrystals was around 32 nm, which was evaluated from the broadening of X-ray diffraction peaks. When the heat-treatment temperature was 600 °C, the crystallite size was almost independent of the heat-treating time, while it increased with time at 800 and 1000 °C. The emission intensity of the $^4I_{13/2} \rightarrow {}^4I_{15/2}$ transition and the lifetime of the $^4I_{13/2}$ level increased with increasing heat-treatment temperature and time. The decrease in the organic residues due to the combustion during the heat treatment at 600 °C and the decrease in the specific surface area induced by the heat treatment at 800 and 1000 °C are responsible for the observed phenomena, i.e., the increase in the emission intensity and lifetime. Quantum efficiencies of Er^{3+} ions in the nanocrystals were also evaluated based on an assumption that the radiative decay rates of the nanocrystals are equal to that of the bulk crystal. The relationship between the quantum efficiency and the specific surface area of the nanocrystals were discussed with a simple model, which led to the conclusion that Er^{3+} ions in the surface region with thickness about 10 nm do not work well as luminescence centers due to the many defects. The Er:YAG nanocrystals prepared by the glycothermal method had emission linewidth broader than the polycrystalline bulk crystal prepared by a solid-state reaction.
© 2004 Published by Elsevier B.V.

PACS: 61.46.+w; 78.55.−m
Keywords: YAG; Nanocrystals; Photoluminescence; Erbium

1. Introduction

Enormous amount of information is transmitted by optical telecommunication. In the wavelength-division-multiplexing (WDM) system, signals with different wavelengths are put together on an optical fiber, and each signal is carried at the same time on its own wavelength. The range of telecommunication wavelengths is dominated by the optical loss of the silica-based transmission fiber. In order to maximize the utilization of this window, various optical amplifiers are proposed and put into practical use. The Er^{3+} is one of the most important active ions, since the wavelength of the $^4I_{13/2} \rightarrow {}^4I_{15/2}$ transition matches the minimum loss region of the silica-based optical fiber. In addition, the quantum efficiency of this transition is usually very high even in oxide materials with high phonon energy. Er^{3+}-doped

* Corresponding authors. Tel.: +81 75 383 2414; fax: +81 75 383 2410
** Tel.: +81 75 753 6832; fax: +81 75 753 6634.
E-mail addresses: west@collon1.kuic.kyoto-u.ac.jp (M. Nishi), stanabe@gls.mbox.media.kyoto-u.ac.jp (S. Tanabe).

0925-3467/$ - see front matter © 2004 Published by Elsevier B.V.
doi:10.1016/j.optmat.2004.08.074

fiber amplifiers (EDFAs) are applied mostly for C (1530–1565 nm) and L (1565–1625 nm) -bands, since in most of materials the emission due to the $^4I_{13/2} \rightarrow {}^4I_{15/2}$ transition covers only these bands.

On the other hand, both the $^4I_{13/2}$ and $^4I_{15/2}$ levels of Er^{3+} in YAG crystal have a large Stark splitting, which leads to the emission even in the U-band (1625–1675 nm) [1,2]. This band is expected to be another candidate for optical telecommunication and there are some researches on the rare-earth-doped U-band optical amplifiers [3,4]. However, it is generally very difficult to make fibers by crystalline materials because of their poor workability. This is one of the reasons why glass materials are used for optical amplifiers. The glass materials have good workability such as fiberizability. We consider that Er-doped YAG precipitated or dispersed glass–ceramics that will have optical properties of the Er:YAG and workability of the glass materials can be excellent candidates for optical amplifiers, especially in the U-band. In addition, they can be transparent if the crystal size is much smaller than the wavelength of incident lights [5–7].

In this report, we focus on the fluorescence properties in telecommunication band for Er:YAG nanocrystals synthesized by a glycothermal reaction [8,9]. In particular, heat treatment was performed for as-prepared Er:YAG nanocrystals, and the effects of heat-treatment temperature and time on the emission intensity of the $^4I_{13/2} \rightarrow {}^4I_{15/2}$ transition and on the lifetime of the $^4I_{13/2}$ level were examined. We also discuss the relationship between quantum efficiency and the size of the nanocrystals using a simple model.

2. Experimental

2.1. Sample preparation

Aluminium isopropoxide (AIP; NacalaiTesque) (25.0 g, 122 mmol), yttrium acetate tetrahydrate (Wako Pure Chemical Industry) (23.5 g, 69.5 mmol), and erbium acetate tetrahydrate (Wako Pure Chemical Industry) (3.7 g, 1.54 mmol) were suspended in 440 ml of 1,4-butanediol (1,4-BG; NacalaiTesque) in a test tube serving as an autoclave liner, and the mixture was placed in a 1 l autoclave. An additional 60 ml of 1,4-BG was placed in the gap between the autoclave wall and test tube. The autoclave was completely purged with nitrogen, heated to the 300 °C at a rate of 2.3 °C min^{-1}, and kept for 2 h. After the assembly was cooled to room temperature, the resulting products were centrifuged. The sediment part of products was repeatedly washed with methanol by mixing and centrifuging (product A). The suspension and all of the washings were gathered, and concentrated ammonium hydroxide was added dropwise until the upper part of the mixture became clear and particles began to settle. The mixture was then centrifuged and washed repeatedly (product B). Heat treatment was performed for the as-prepared specimen at 600, 800, and 1000 °C. The initial heating rate up to the desired hold temperature was 100 °C/h.

2.2. Measurements

X-ray powder diffraction (XRD) measurements were performed using a Cu Kα radiation (XRD-6000, Shimazu). The XRD pattern of a standard Si crystal was also measured in order to estimate the instrumental broadening. Field-emission scanning electron microscope (FE-SEM) (JEOL JSM-6700F) was used to observe the morphology of the as-prepared and calcined particles and also to evaluate the particle size. Thermogravimetric analysis was carried out for the as-prepared nanocrystals (Rigaku TG8120). Fluorescence spectra were measured in the range of 1380–1750 nm with a computer-controlled monochromator (Nikon, G-250), a PbS photodiode detector (Hamamatsu, P4638), and a lock-in-amplifier (NF Electronic Instruments, LI-570A). A diode laser of 970 nm (SDL-6362-P1) was used as the excitation source. The fluorescence decay curve of the $^4I_{13/2}$ level was also measured with an InGaAs photodiode detector ($f = 160$ kHz; Electro-Optical System, IGA-010-H) and a digital oscilloscope (LeCroy LS140). The diode laser of 970 nm was modulated to pulse with a function generator for the decay measurements. The lifetime was determined by the least-squares fitting of a single exponential function to the obtained decay curve. The sample holder employed for X-ray diffraction measurements was also used for the fluorescence measurements. A silicon wafer was used as the filter to cut off the scattering light of the exciting light.

2.3. Analyses

The linewidth of X-ray diffraction peaks gives us the information about crystallite size. The crystallite size was estimated using the following equation:

$$\frac{\beta \cos\theta}{\lambda} = \frac{0.9}{D} + \frac{2\eta \sin\theta}{\lambda}, \quad (1)$$

where D is the crystallite size, λ is the wavelength of X-ray, θ is the diffraction angle, η is inhomogeneous strain, and $\beta = \beta_{exp} - \beta_{app} = \beta_{crys} + \beta_{strain}$. Here, β_{exp} is a full-width at half-maximum (FWHM) of diffraction line, β_{app} is the instrumental broadening width, and β_{crys} and β_{strain} are FWHMs caused by the effect of crystallite size and inhomogeneous strain, respectively. For this estimation, β_{exp} was obtained by assuming that the diffraction peak is expressed as a Gaussian distribution function, and β_{app} was determined by the analysis of diffraction lines of a standard Si crystal. Thus, the crystallite size can be extracted by extrapolating Eq. (1) to $\theta = 0$.

3. Results

As described in the experimental section, the product obtained by the glycothermal synthesis did not completely sediment by centrifuging. Therefore, the suspension was sedimented by the addition of ammonia solution. The XRD patterns of products A and B (see experimental section) are shown in Fig. 1. The XRD lines of product B can be assigned to YAG (JCPDS card No. 33–40), while those of product A include some undefined impurity phases in addition to YAG. Only product B was thus subjected to the heat treatment, and the fluorescence properties were examined. Fig. 2 shows the thermogravimetric curve for the as-prepared nanocrystals. Weight loss was observed continuously even at the temperature higher than 400 °C. Fig. 3 plots $\beta\cos\theta/\lambda$ vs. $\sin\theta/\lambda$ for the X-ray diffraction lines of the as-prepared Er:YAG nanocrystals. The straight line represents the least-squares fitting of Eq. (1) to the data points. From the extrapolation of Eq. (1) to $\theta = 0$, the crystallite size of the as-prepared nanocrystals was estimated to be 32 nm, which is almost equal to the crystallite size of the YAG nanocrystals as reported previously [8]. Fig. 4 depicts a FE-SEM image of the as-prepared nanocrystals. The particle size observed was around 30 nm, which is also consistent with the result in Ref. [8]. The dependence of crystallite size on the heat-treatment time is shown in Fig. 5. The heat treatment was performed at 600, 800, and 1000 °C. The crystallite size was almost independent of the heat-treatment time at 600 °C, while it increased with time at 800 °C and 1000 °C. In Fig. 6

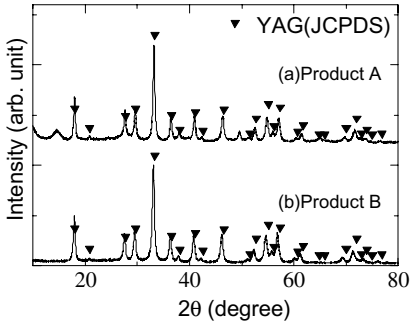

Fig. 1. XRD patterns of (a) the product A and (b) the product B prepared by the glycothermal reaction.

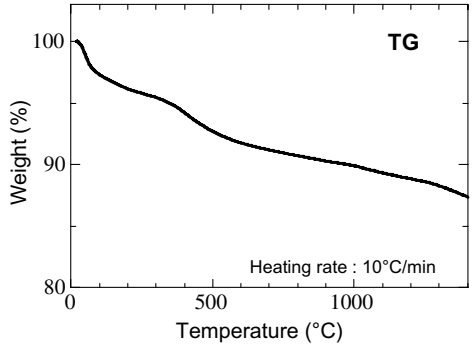

Fig. 2. A thermogram for the Er:YAG nanocrystals prepared by the glycothermal reaction. The measurement was performed for the as-prepared specimen.

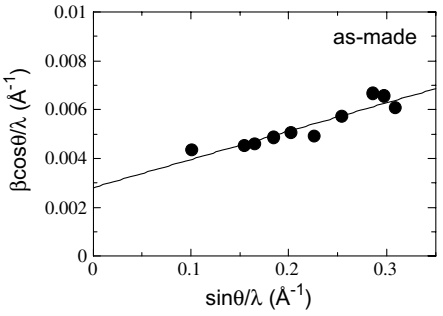

Fig. 3. The plot of $\beta\cos\theta/\lambda$ vs. $\sin\theta/\lambda$ for the diffraction lines of as-synthesized Er:YAG nanocrystal. The straight line represents least-squares fitting of Eq. (1).

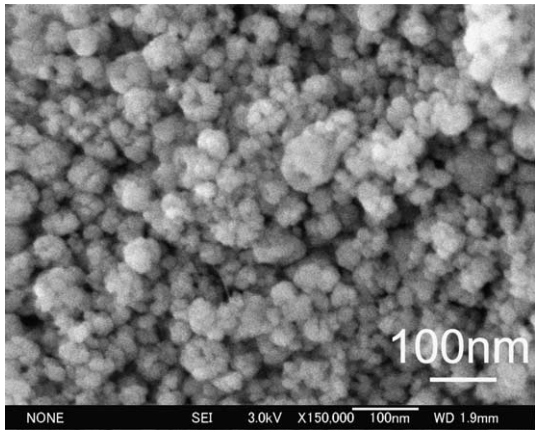

Fig. 4. FE-SEM image of the Er:YAG nanocrystals prepared by the glycothermal reaction. The observation is made for the as-prepared specimen.

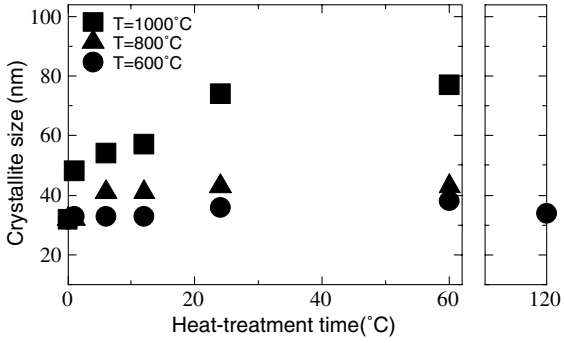

Fig. 5. The dependence of the crystallite size on the heat-treatment time. The heat treatment was performed at 600, 800, and 1000 °C.

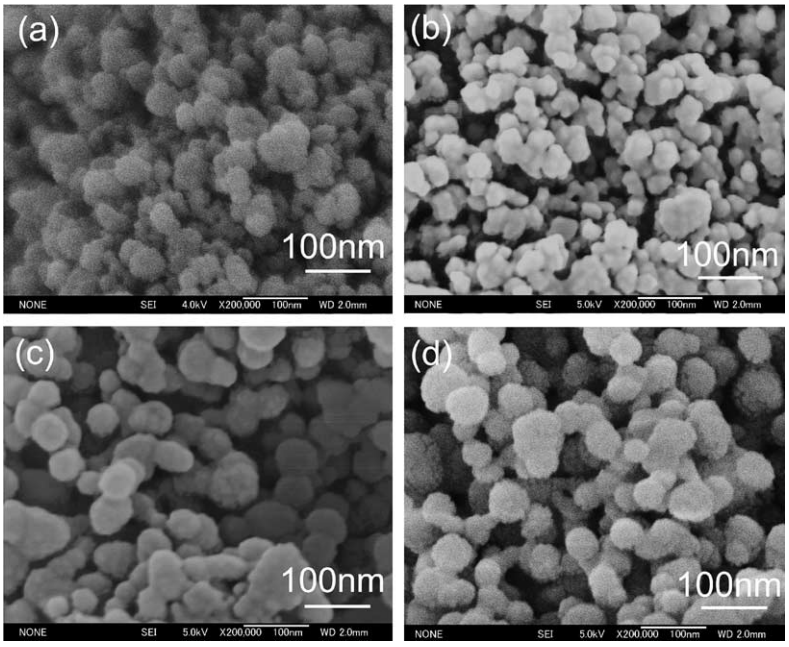

Fig. 6. FE-SEM images of the Er:YAG nanocrystals heat-treated at (a) 800 °C for 6 h, (b) 800 °C for 24 h, (c) 1000 °C for 6 h, and (d) 1000 °C for 24 h.

are shown FE-SEM images of the nanocrystals heat-treated at 800 °C and 1000 °C for 6 and 24 h. It is evident that the particle size increases as the heat-treatment temperature is increased. From Figs. 5 and 6, it can be seen that the particle size is comparable with the crystallite size even when the heat treatment was performed at 1000 °C.

Fig. 7 shows the emission spectra due to the $^4I_{13/2} \rightarrow {}^4I_{15/2}$ transition of Er^{3+} in YAG nanocrystals heat-treated at 600 °C, 800 °C, and 1000 °C for 12 h, which are normalized at the peak around 1530 nm. For comparison, the spectrum of the polycrystalline bulk Er:YAG prepared by a solid-state reaction is also shown. The finger pattern in the figure denotes the possible emission wavelengths calculated using the values of Stark splitting of both the $^4I_{13/2}$ and $^4I_{15/2}$ levels of Er^{3+} [1]. The peak positions of the emission spectra observed in nanocrystals agree with the calculated emission wavelengths, indicating that Er^{3+} is located at the Y^{3+} site of the crystalline YAG phase. In addition, the emission linewidths of the nanocrystals are broader than that of the bulk crystal. The dependence of the integral emission intensity on the heat-treatment temperature and time is shown in Fig. 8. The integral emission intensity increased with increasing heat-treatment time when the heat-treatment temperature was

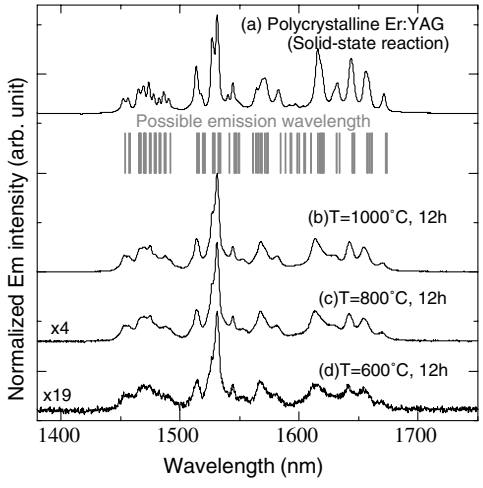

Fig. 7. Normalized emission spectra due to the $^4I_{13/2} \rightarrow {}^4I_{15/2}$ transition of Er^{3+} in (a) polycrystalline bulk YAG prepared by solid-state-reaction and YAG nanocrystals heat-treated at (b) 1000, (c) 800, and (d) 60 °C for 12 h. The finger pattern denotes the possible emission wavelengths calculated using the values of Stark splitting of $^4I_{13/2}$ and $^4I_{15/2}$ levels of Er^{3+} [1].

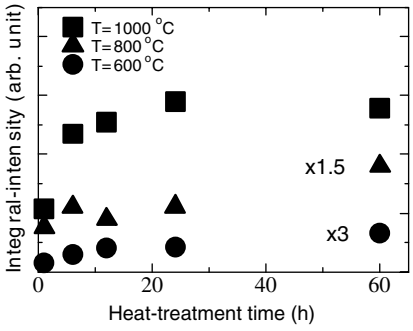

Fig. 8. The dependence of the integral intensity of the emission due to the $^4I_{13/2} \rightarrow {}^4I_{15/2}$ transition of Er^{3+} in the YAG nanocrystals on the heat-treatment time. The heat treatment was performed at 600, 800, and 1000 °C.

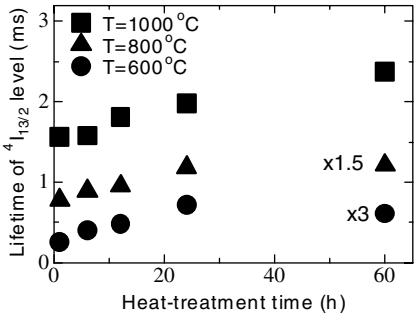

Fig. 9. The dependence of the lifetime of the $^4I_{13/2}$ level of Er^{3+} in the YAG nanocrystals on the heat-treatment time. The heat treatment was performed at 600, 800, and 1000 °C.

fixed. Also, it is found that the emission intensity as a function of the heat-treatment time becomes more rapidly intense when the heat-treatment temperature is higher.

The emission intensity is proportional to the lifetime of the initial level provided that the radiative transition probability is not changed. The lifetimes of the $^4I_{13/2}$ level are shown in Fig. 9 for the heat-treated nanocrystals. In analogy with the case of the integral emission intensity, the lifetime depended largely on the heat-treatment conditions. In other words, the lifetime increased with increasing heat-treatment temperature and time.

4. Discussion

4.1. Emission linewidth

As shown in Fig. 7, the emission linewidths of Er:YAG nanocrystals were broader than that of the polycrystalline bulk crystal. It is quite likely that this line-broadening is derived from the large inhomogeneity around Er^{3+}. It was previously reported that the lattice of the YAG nanocrystals prepared by the glycothermal reaction is distorted [8,9]. The large specific boundary area of the crystallites may also have effect on the line-broadening, since the lattice distortion is expected to occur in the boundary of crystallites. The line-broadening can be useful for the gain flatness at around optical-telecommunication wavelengths if we take the application of the material to WDM optical amplifiers into consideration.

4.2. Lifetime

The lifetime of the $^4I_{13/2}$ level is expressed as the following equation:

$$\tau_f = \frac{1}{A + \sum W_{NR}}, \tag{2}$$

where A (s^{-1}) is the radiative decay rate and equal to the spontaneous emission probability of the $^4I_{13/2} \rightarrow {}^4I_{15/2}$ transition in the present case, and $\sum W_{NR}$ is the non-radiative decay rate. As will be shown below, it is good approximation that the radiative decay rate A (s^{-1}) of the nanocrystals does not vary with the heat treatment and is equal to that of the bulk crystal.

The spontaneous emission probability between an initial manifold $|(SL)J\rangle$ and a final manifold $|(S'L')J'\rangle$ is expressed as follows:

$$A[(SL)J;(S'L')J'] = \frac{64\pi^4 e^2}{3h(2J+1)\lambda^3} \times \left\{ \frac{n(n^2+2)^2}{9} S^{ed} + n^3 S^{md} \right\}, \tag{3}$$

where e is the elementrary charge, h the Planck constant, n the refractive index, and λ the mean wavelength. The S^{ed} and S^{md} are the line strength for the electronic dipole transition and for the magnetic dipole transition, respectively. The S^{md} is dominated only by the angular momentum quantum numbers of both the initial and terminal states and is independent of the local structure around Er^{3+}, while S^{ed} depends on it. The S^{ed} of the $^4I_{13/2} \rightarrow {}^4I_{15/2}$ transition of Er^{3+} is given by

$$S^{ed}[{}^4I_{13/2};{}^4I_{15/2}] = 0.0195\Omega_2 + 0.1173\Omega_4 + 1.4316\Omega_6, \tag{4}$$

where Ω_t ($t = 2, 4, 6$) are the intensity parameters which contain the effects of crystal-field terms, radial integrals of an electron, and so on. One can see from Eq. (4) that the S^{ed} of the $^4I_{13/2} \rightarrow {}^4I_{15/2}$ transition of Er^{3+} is dominated by the Ω_6 parameter. It is well known that the three Ω_t parameters are dependent on the local structure around rare-earth ions; the Ω_2 value is sensitive to the asymmetry of ligand field [10], while the Ω_4 and Ω_6 values, which are less sensitive to the local environment than Ω_2 value, are related to the bond covalency [11,13]. Judging from the fact that Er^{3+} ions in the YAG nanocrystals occupy the Y sites, the degree of bond covalency is not so largely changed between nanocrystals and bulk crystals, although it is anticipated that the inhomogeneity of the nanocrystals (see Section 4.1) has some significant influences on Ω_2 value [10]. Here, it should be noted that the value of Ω_2 is at most comparable to that of Ω_6 in many crystalline and amorphous materials [11–13], and does not so significantly contribute to the radiative decay rate. We thus deduce that the difference in the radiative decay rates that depend mainly on Ω_6 is negligibly small between the nanocrystals heat-treated under various conditions and bulk crystal. Although the refractive indices of the nanocrystals may be slightly different from that of bulk crystal owing to the larger inhomogeneity, the difference is also considered to be small. Then, the lifetimes of the $^4I_{13/2}$ level of Er^{3+} in nanocrystals is approximately described as

$$\tau_{f,i} = \frac{1}{A_i + \sum W_{NR,i}} \approx \frac{1}{A_{bulk} + \sum W_{NR,i}}, \tag{5}$$

where the subscript i denotes the nanocrystals heat-treated under a given condition (time and temperature). A_{bulk} corresponds to the radiative decay rate of the polycrystalline bulk Er:YAG prepared by the solid-state reaction.

The increase in the lifetime with the increase in heat-treatment temperature can be thus attributed to the decrease in the non-radiative decay rate. Fig. 10 shows the dependence of the lifetime on the crystallite size. When as-prepared nanocrystals were heat-treated at 800 and 1000 °C, the lifetime monotonically increased as the crystallite size is increased, although it was independent of the crystallite size when the heat-treatment temperature was 600 °C. Based on these tendencies, we consider the different origins of the lifetime increase between heat treatment at 600 °C and those at 800 and 1000 °C. First, we discuss the increase in the lifetime under the heat treatment at 600 °C. According to the previous study, there always remain a large amount of organic residues because of the simple adsorption on the product surface and/or the covalent bonding to the surface oxygen atoms of the particles [8,9,14–16]. In the present case, the presence of the organic components is confirmed from the thermogravimetric curve as shown in Fig. 2, where the weight loss due to the combustion of organic components is still observed continuously at temperatures higher than 400 °C. It is quite likely that these organic residues can work as quenching centers. The increase in the lifetime with heat-treatment time at 600 °C is thus caused by the decrease in the organic residues due to the combustion. Next is for the increase in the lifetime with heat-treatment time at 800 and 1000 °C, which is accompanied with the increase in crystallite size. The previous studies on YAG nanocrystals derived by the glycothermal reaction revealed that the crystallite size of nanocrystals matches the crystal grain size, indicating they were precipitated as a single crystal phase [8]. This can also be true in the case of present Er^{3+}-doped YAG nanocrystals, since the difference in ionic radii between Er^{3+} and Y^{3+} is less than 1 percent, so the Er^{3+} and Y^{3+} sites in a given crystal structure are

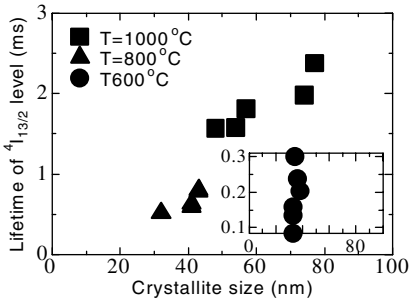

Fig. 10. Variation of the lifetime of the $^4I_{13/2}$ level of Er^{3+} in YAG nanocrystals heat-treated at 600, 800, and 1000 °C with the crystallite size.

almost identical to each other from the viewpoint of crystallography. The FE-SEM photograph in Fig. 4 confirms that the crystal grain size is around the crystallite size. The increase in the crystallite size therefore means the increase in the crystal grain size, because the coupling from crystallite to crystallite is required for the grain growth. The increase of the crystal grain size under heat treatment, as shown in Fig. 6, leads to the decrease of the specific surface area in which many defect centers exist. Thus, it is reasonable to consider that parts of these defects can work as quenching centers, since some defects adsorb or bind to H_2O molecules in air, leading to the generation of –OH bonds with high vibration energy (~3600 cm^{-1}). The non-radiative decay rate of Er^{3+} at the surface of the crystal grain can be so large that the contribution from the radiative decay rate is negligibly small. As a consequence, the decrease in the specific surface area of the nanocrystals is responsible for the increase in the lifetime with heat-treatment time at 800 and 1000 °C.

4.3. Quantum efficiency

The quantum efficiency of the $^4I_{13/2} \rightarrow {}^4I_{15/2}$ transition of Er^{3+} is described as

$$\eta = \frac{A}{A + \sum W_{NR}} = \tau_f A. \tag{6}$$

Using Eq. (5), we can obtain that

$$\eta_i = \frac{A_i}{A_i + \sum W_{NR,i}} \approx \frac{A_{bulk}}{A_{bulk} + \sum W_{NR,i}} = \tau_{f,i} A_{bulk}. \tag{7}$$

In order to estimate the quantum efficiencies of the nanocrystals, that of the bulk crystal is required. $\sum W_{NR}$ of the prepared polycrystalline bulk Er:YAG can be almost equal to the multi-phonon decay rate W_p and it is presumed that W_p of the $^4I_{13/2}$ level of Er^{3+} in the bulk crystal is less than 1 s^{-1}, which is derived from the large energy gap (~6500 cm^{-1}) between the $^4I_{13/2}$ and the next lower level, that is, the $^4I_{15/2}$ level, and the relatively low phonon energy of the YAG crystal (~700 cm^{-1}) [17–19]. The lifetime of the $^4I_{13/2}$ level for the prepared polycrystalline bulk Er:YAG was 5.6 ms. Therefore, in the case of the bulk crystal, W_p can be disregarded compared with A_{bulk}. Then, A_{bulk} approximately corresponds to the reciprocal of the lifetime:

$$A_{bulk} \approx \frac{1}{\tau_{f,bulk}}. \tag{8}$$

Based on Eqs. (7) and (8), we estimated the quantum efficiencies of the nanocrystals (see Fig. 11). The highest value of the quantum efficiency was about 40% which was obtained for the Er:YAG nanocrystals heat-treated at 1000 °C for 60 h.

As discussed in Section 4.2, the non-radiative decay rate of Er^{3+} at the surface of the crystal grain is pre-

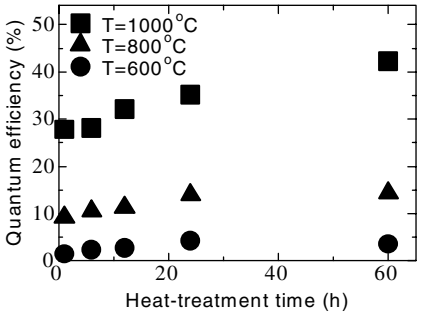

Fig. 11. The dependence of the estimated quantum efficiency of the $^4I_{13/2} \rightarrow {}^4I_{15/2}$ transition of Er^{3+} in the YAG nanocrystals on the heat-treatment time. The heat treatment was performed at 600, 800, and 1000 °C.

sumed to be so large that the contribution from the radiative decay rate is negligible. Based on this assumption, a simple model is given as follows. The shape of a nanocrystal is approximated as a sphere. Although the spatial distribution of the quantum efficiency in the sphere can be continuous, the discrete one is assumed. More specifically, the quantum efficiency of the surface region with thickness d (nm) is approximated as 0 (%) and that of the other region is as 100 (%). Then, the relationship between the total quantum efficiency and crystal grain size can be described by

$$\eta = \frac{V_{\text{lum}}}{V} = \frac{8\left(\frac{D}{2} - d\right)^3}{D^3}, \tag{9}$$

where D (nm) is the diameter of the crystal sphere, namely, the crystal grain size, V is the total volume of the crystal sphere, and V_{lum} is the volume of the region of $\eta \approx 100(\%)$. In Fig. 12, the solid curve represents the least-squares fitting of Eq. (9) to the experimental results. Here, the crystallite size was used instead of the crystal grain size, since both the sizes were comparable to each other as seen from Figs. 5 and 6. The agreement between the fitted curve and

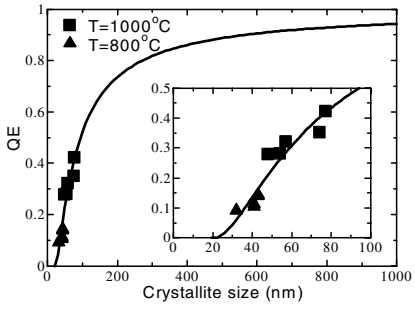

Fig. 12. The relation between the estimated quantum efficiency η and the crystallite size D. The solid curve represents least-squares fitting of Eq. (9) to the experimental data. In the inset is enlarged the plot of η vs. D.

experimental data is fairly good, indicating that the volume with thickness of 10 nm on the surface of nanocrystals is almost non-luminescent. The region of $d = 10$ nm corresponds to the 96% and 58% of the total volume for the nanocrystals with the size of 30 nm and 80 nm, respectively. The considerably large volume of $\eta \approx 0$ region may be derived from many defects growing in the direction of the crystal growth in the glycothermal reaction [9]. The surface with markedly uneven dramatically increases the specific surface area. Owing to the large specific surface area, the surface conditions can determine the fluorescence properties of the nanocrystals. When we take the application of Er:YAG nanoparticles to the optical amplifier into consideration, packing with glass materials will be necessary, since the nanoparticles easily aggregate and do not have transparency. The increase in quantum efficiency of nanocrystals are expected by glass packing, since the chemical bonds of –M–O–M_1–(M = Er, Y, or Al, and M_1 is a cation of the glass) will be formed to prevent the surface of the nanocrystals from being exposed to air (Improvement in quantum efficiency under a constant nanoparticle size). In addition, when nanoparticles are packed with glass materials whose refractive indices are the same as that of nanoparticles, transparent composites can be obtained even if the particle size is as large as 80 nm (Control of light scattering by the bigger nanoparticles).

5. Conclusions

We investigated the optical-telecommunication-band fluorescence properties of Er:YAG nanocrystals prepared by a glycothermal reaction. The emission intensity of the $^4I_{13/2} \rightarrow {}^4I_{15/2}$ transition and the lifetime of the $^4I_{13/2}$ level increased with heat-treatment time and temperature. The variation of the spontaneous emission probability with heat treatment is deduced to be negligibly small, so the increase in the emission intensity and lifetime can take place as a result of the decrease in the non-radiative decay rate. The origin of the decrease in the non-radiative decay rate at the heat-treatment temperature of 600 °C is different from that of 800 and 1000 °C. At 600 °C, the non-radiative decay rate decreases mainly due to the combustion of the organic residues that act as quenching centers, while at 800 and 1000 °C, the decrease in the specific surface area causes the non-radiative decay rate to decrease. The quantum efficiency as high as 40% is achieved in nanocrystals heat-treated at 1000 °C for 60 h. The emission linewidths of the nanocrystals were broader than that of the bulk crystal, presumably due to the increase in the disorder or

inhomogeneity by the presence of the structural imperfection and lattice distortion.

References

[1] A.A. Kaminskii, Crystalline Lasers: Physical Processes and Operating Schemes, CRC Press, New York, 1996 (Chapter 2).
[2] M. Nishi, S. Tanabe, K. Fujita, K. Hirao, Trends in Optics and Photonics, in: Optical Amplifiers and their Applications, vol. 92, 2003, p. 45.
[3] Y.G. Choi, K.H. Kim, B.J. Park, J. Heo, Appl. Phys. Lett. 78 (9) (2001) 1249.
[4] T.H. Lee, J. Heo, International Symposium on Photonic Glasses 2002 Abstract Shanghai, October 2002, p. 20.
[5] P.A. Tick, N.F. Borrelli, L.K. Cornelius, M.A. Newhouse, J. Appl. Phys. 78 (11) (1995) 6367.
[6] P.A. Tick, Opt. Lett. 23 (24) (1998) 1904.
[7] M.J. Dejneka, J. Non-Cryst. Solids 239 (1998) 149.
[8] M. Inoue, H. Otsu, H. Kominami, T. Inui, J. Alloys Compd. 226 (1995) 146.
[9] M. Inoue, T. Nishikawa, H. Otsu, H. Kominami, T. Inui, J. Am. Ceram. Soc. 81 (1998) 1173.
[10] C.K. Jørgensen, B.R. Judd, Mol. Phys. 8 (1964) 281.
[11] S. Tanabe, T. Ohyagi, N. Soga, T. Hanada, Phys. Rev. B 46 (1992) 3305.
[12] A.A. Kaminskii, Crystalline Lasers: Physical Processes and Operating Schemes, CRC Press, New York, 1996, Chapter 3.
[13] S. Tanabe, T. Ohyagi, S. Todoroki, H. Hanada, N. Soga, J. Appl. Phys. 73 (12) (1993) 8451.
[14] M. Inoue, Y. Kondo, T. Inui, Inorg. Chem. 27 (1988) 215.
[15] H. Kominami, M. Inoue, T. Inui, Catal. Today 16 (1993) 309.
[16] M. Inoue, H. Kominami, T. Inui, J. Chem. Soc., Dalton Trans. (1991) 3331.
[17] T. Miyakawa, D.L. Dexter, Phys. Rev. B 1 (1970) 2961.
[18] C.B. Layne, W.H. Lowdermilk, M.J. Weber, Phys. Rev. B 16 (1977) 10.
[19] G.M. Zverev, G.Y. Kolodnyi, A.M. Onishchenko, Sov. Phys. JETP 33 (1971) 497.